Nanoscale

ROYAL SOCIETY OF CHEMISTRY

PAPER

Check for updates

Cite this: *Nanoscale*, 2021, **13**, 9732

Intrinsic effect of interfacial coupling on the high-frequency intralayer modes in twisted multilayer $MoTe_2$†

Yu-Chen Leng,[a,b] Miao-Ling Lin,[a] Yu Zhou,[c] Jiang-Bin Wu,[a] Da Meng,[a] Xin Cong,[a,b] Hai Li[c] and Ping-Heng Tan*[a,b,d]

Received 27th February 2021,
Accepted 17th April 2021

DOI: 10.1039/d1nr01309b

rsc.li/nanoscale

The interfacial coupling at the interface makes the van der Waals heterostructures (vdWHs) exhibit many unique properties that cannot be realized in its constituents. Such a study usually starts with a twisted stack of two flakes exfoliated from the same layered materials to form twisted multilayers, in which the impact of interfacial coupling on the low-frequency interlayer modes had been well understood. However, it is not clear how interfacial coupling affects the high-frequency intralayer modes of twisted multilayers. Herein, we perform high-resolution resonance Raman spectroscopy of the high-frequency intralayer modes in twisted multilayer $MoTe_2$ (tMLM). All the Davydov entities of the out-of-plane intralayer mode are observed and distinguished at 4 K. It is found that the out-of-plane intralayer modes in tMLM are sensitive to its interfacial layer-breathing coupling so that the out-of-plane intralayer modes in tMLM do not show a direct relationship with those of the two constituents. However, the case is quite different for the in-plane intralayer modes in tMLM, whose spectral profile can be fitted by those of the corresponding modes of its constituents. This indicates that the in-plane intralayer modes are localized within the constituents in tMLM because of its negligible interfacial shear coupling at the interface. All the results can be well understood using the vdW model in which only the nearest neighbor interlayer/interfacial interaction is taken into account. This work directly builds the relationship between the Davydov splitting of the high-frequency intralayer vibrations and the low-frequency interlayer vibrations in tMLM, which can be further extended to other twisted materials and the related vdWHs.

1. Introduction

The atoms within each layer in two-dimensional transition metal dichalcogenide (TMD) flakes are joined together by covalent bonds, while the interlayer coupling of van der Waals (vdW) interactions keeps the layers together. The vdW interactions dominate the interlayer modes[1] in TMD flakes, which serve as persuasive fingerprints for their interlayer coupling.[2] The interlayer interaction also leads to the observation of Davydov splitting of the intralayer modes in 2H-MoS_2.[3] In principle, there are N Davydov entities of the high-frequency intralayer mode in 2H-stacked N-layer ($N > 1$) flakes.[4–6] The force constant model[4] and vdW model[5] had been proposed to explain frequency evolution of the intralayer modes with N. The force constant model was used to calculate the frequency of each Davydov component of TMD flakes,[4,6–8] in which interactions up to the second nearest neighbor and surface effects were included. The force constants per unit area are obtained by fitting the experimental frequencies of the A_{1g}^2 (or A_1') modes at ~172 cm^{-1}. However, the small splitting (~1 cm^{-1}) of the A_{1g}^1 (or A_1') modes at ~290 cm^{-1} in N-layer $MoTe_2$ were attributed to the surface effects, but not Davydov splitting. The surface effects were also claimed to dominate the small splitting of the E_g (or E') modes at 235 cm^{-1}.[4] In fact, the frequency of the intralayer modes in N-layer TMD flakes is not only dominated by the interlayer and intralayer force constants, but also by the long-range Coulomb interaction and short-range multipolar interactions.[3–5,9,10] This is why each kind of TMD flake exhibits specific N-dependent frequency difference between A_{1g}^2 (or A_1') and E_g (or E') modes,

---

[a] State Key Laboratory of Superlattices and Microstructures, Institute of Semiconductors, Chinese Academy of Sciences, Beijing 100083, China. E-mail: phtan@semi.ac.cn

[b] Center of Materials Science and Optoelectronics Engineering & CAS Center of Excellence in Topological Quantum Computation, University of Chinese Academy of Sciences, Beijing 100049, China

[c] Key Laboratory of Flexible Electronics and Institute of Advanced Materials, Jiangsu National Synergetic Innovation Center for Advanced Materials, Nanjing Tech University, 30 South Puzhu Road, Nanjing 211816, China

[d] Beijing Academy of Quantum Information Science, Beijing 100193, China

† Electronic supplementary information (ESI) available: Further details of the diatomic chain model. See DOI: 10.1039/d1nr01309b

such as MoS_2, WS_2, WSe_2, $MoTe_2$ and $MoSe_2$.[4,5,11–13] For the vdW model, the interlayer coupling is considered as a first-order perturbation, which is responsible for the Davydov splitting between Davydov entities in *N*-layer flakes, while other factors, such as long-range Coulomb interactions and short-range multipolar interactions, may result in the frequency difference between uncoupled entities, *e.g.*, the lowest-frequency A_{1g}^2 (or A_1') modes in each *N*-layer flake. The vdW model bridges the relationship between the Davydov splitting of the intralayer modes and the frequency of the interlayer modes,[5] and well reproduces the Davydov splitting of Davydov entities in $MoTe_2$ flakes,[5] which had been extended to other TMD flakes, such as $MoSe_2$ and MoS_2 flakes.[13] To date, the two models have been widely used to understand the frequency of high-frequency intralayer modes in TMD flakes and other two-dimensional flakes although their physical origins are quite different. Therefore, it is an essential issue to further uncover the nature of interlayer coupling in TMD flakes.

In comparison with the 2H-stacked *N*-layer TMD flakes, twisted TMD flakes assembled by vertically stacking two TMD flakes together with a twist angle provide multiple degrees of freedom, such as layer thickness and twist angle at the interface, to engineer their optical and electronic properties. The effects of interfacial coupling on the interlayer modes have been clearly demonstrated, where the negligible interfacial shear (S) coupling leads to the localization of the S modes within its constituents and the significant layer-breathing (LB) coupling gives rise to collective vibration of all the stacking layers for the LB modes.[14–16] Frequency shift had been observed in twisted TMD flakes.[17] However, Davydov entities of the intralayer modes in twisted TMD flakes have not been explored yet. Revealing the effect of interlayer/interfacial coupling on intralayer vibrations in twisted TMD flakes will fundamentally enrich our understanding of the properties of the intralayer modes in these systems.

Because the Davydov splitting in 2H-stacked *N*-layer $MoTe_2$ flakes had been well studied, here, we performed high-resolution resonance Raman spectroscopy of twisted multilayered $MoTe_2$ (tMLM) at low temperature to reveal the effect of interfacial coupling on its Davydov splitting. Under these experimental conditions, all the Davydov entities of the out-of-plane intralayer modes in tMLM and the corresponding 2H-stacked *N*-layer $MoTe_2$ (*N*LM, $N > 1$) were observed. The Davydov splitting of the intralayer modes in tMLM is well reproduced by the vdW model. The smaller Davydov splitting of the out-of-plane intralayer modes in tMLM is attributed to its weaker interfacial LB coupling than the interlayer LB coupling within *N*LM. In addition, the spectral profile of the in-plane intralayer modes in tMLM is the sum of those from the corresponding constituents due to its negligible interfacial S coupling. The results show that without any fitting parameters, the observed Davydov splitting of the two out-of-plane intralayer modes in tMLM can be quantitatively described by the vdW model based on the frequencies of the corresponding LB modes.

2. Experimental

Sample preparation

The t(*m*+*n*)LM are prepared by assembling *m*-layer $MoTe_2$ (*m*LM, $m \geq 1$) and *n*LM ($n \geq 1$) together *via* a wet transfer method.[18] The *n*LM flakes were prepared on 90 nm SiO_2/Si substrates by the mechanical exfoliation method. The number of layers of the *n*LM flake was measured by low-frequency Raman spectroscopy. Then 3.0 wt% polymethyl methacrylate (PMMA) in dichloromethane solution was spin-coated on the *m*LM flake at 3000 rpm to generate the PMMA film, which was sequentially covered by a polydimethylsiloxane (PDMS) film. After this, the PDMS/PMMA/*n*LM film was separated from the substrate with a drop of water and then stacked on top of other *m*LM flakes by using a micromanipulator under an optical microscope to obtain the PDMS/PMMA/*n*LM/*m*LM structure. The PDMS film was peeled off with a hot plate at 50 °C to form the PMMA/*n*LM/*m*LM structure, and then the PMMA film was removed with anhydrous dichloromethane at 50 °C. Finally, the *n*LM/*m*LM (t(*m*+*n*)LM) sample was annealed at 200 °C under an Ar atmosphere for one hour.

SHG measurements

The SHG measurement was performed in a reflection geometry using normal incidence excitation. The pump radiation of 880 nm was supplied by a fs-Ti:Sapphire Laser operating at an 80 MHz repetition rate. The pulse is of 140 ± 20 fs duration. A polarizer was placed in the incident path, and an analyzer was allocated before the spectrometer to select the polarization components of the SHG radiation lying parallel to the polarization of the pump beam. The samples were placed on a rotating platform and rotated to obtain the orientational dependence of the SHG response. The signal was detected using a liquid-nitrogen-cooled charge-coupled device (CCD). The average laser power was kept below 150 μW to avoid sample heating.

Raman measurements

Raman spectra were measured using 647 nm excitation from a Kr^+ laser at room temperature (RT) and 4 K in a helium-cooled cryostat (Montana Instruments), with Raman signal collected by a Jobin–Yvon HR800 micro-Raman system equipped with a liquid-nitrogen-cooled CCD and a 50× objective (numerical aperture = 0.45). A 2400 lines per mm grating was used in the Raman measurements, where the corresponding spectral resolution is 0.17 cm^{-1} per CCD pixel. The laser plasma lines were removed by Bragg-volume-grating based bandpass filters from OptiGrate Corp. Measurement down to 5 cm^{-1} was achieved using three BragGrate notch filters from OptiGrate Corp. with an optical density of 3 and with a full width at half maximum of 5–10 cm^{-1}. The laser power was kept below 150 μW to avoid sample heating.

3. Results and discussion

By vertically assembling a 2H-stacked *m*LM and *n*LM flakes together, an (*m*+*n*)-layer system is formed. Hereafter, we denote it as t(*m*+*n*)LM. Because of the three-fold rotational symmetry of the lattice structure and the lack of centrosymmetry,[19] odd *N*-layer MoTe$_2$ (O*N*LM) exhibits an evident second harmonic response dependent on the crystallographic orientation. Therefore, the twist angle of t(*m*+*n*)LM can be determined by the orientational dependence of the second-harmonic generation (SHG) of its two O*N*LM constituents (see Experimental). Because of the small Davydov splitting of the out-of-plane intralayer modes in *N*LM, a Raman system with ~0.17 cm^{-1} per CCD pixel at 647 nm is used to obtain high-resolution Raman spectra of *N*LM and t(*m*+*n*)LM at 4 K and RT (see Experimental), where the 647 nm excitation is utilized to excite the corresponding resonance Raman spectroscopy with the B′ exciton.[5,20]

We firstly performed Raman measurement on 4LM, t(1+3)LM and its constituents (1LM and 3LM). The optical image of the t(1+3)LM is depicted in Fig. 1(a). The twist angle between the 1LM and 3LM constituents in t(1+3)LM is 9.4°, as indicated in Fig. 1(b). The resonance Raman spectra of 1LM, 3LM, 4LM and t(1+3)LM at RT are plotted in Fig. 1(c). In principle, there are $N-1$ LB and $N-1$ doubly degenerate S modes in *N*LM ($N > 1$), which can be denoted as the LB$_{N,N-j}$ and S$_{N,N-j}$ modes[2] ($j = N-1, N-2, \ldots, 1$), respectively. The LB$_{N,1}$ and S$_{N,1}$ modes are the LB and S modes with the highest frequencies, respectively. No interlayer mode is observed in 1LM. According to the symmetry analysis of *N*LM,[21] the Raman-active modes can be identified, S$_{3,1}$ and LB$_{3,2}$ in 3LM, S$_{4,1}$, LB$_{4,1}$ and LB$_{4,3}$ in 4LM. All the modes are experimentally observed, as shown in Fig. 1(c).

In t(1+3)LM, four Raman peaks are observed in the low-frequency region. According to their frequencies and peak widths, the sharp peak at 23 cm^{-1} corresponds to the S$_{3,1}$ modes of its 3LM constituent, but not the S modes of 4LM that has the same number of layers as t(1+3)LM. This indicates that the interfacial S coupling at the twist interface of t(1+3)LM is so weak that its S mode is localized within its 3LM constituent. The other three peaks belong to the LB modes according to their broader profiles, and are assigned to LB$_{4,3}$, LB$_{4,2}$ and LB$_{4,1}$ with increasing peak positions. Indeed, the frequency of the corresponding modes ω(LB$_{4,3}$) and ω(LB$_{4,1}$) in t(1+3)LM is slightly different from those of the corresponding modes in 4LM. The LB$_{4,2}$ mode, Raman inactive in 4LM, is observed in t(1+3)LM due to its low lattice symmetry. The frequencies of the LB modes in TMD flakes and the corresponding vdW heterostructures (vdWHs) can be well described by the linear chain model (LCM).[1,15,16,22] Here, we apply the LCM to t(1+3)LM and $\alpha^{\perp}$(I) can be treated as a fitting parameter. ω(LB$_{4,3}$) and ω(LB$_{4,1}$) in t(1+3)LM at RT can be well fitted by $\alpha^{\perp}(\mathrm{I}) = 5.06 \times 10^{19}$ N m^{-3}, which is strong enough to generate the collective vibrations of all the stacking layers in t(1+3)LM, similar to other twisted 2DMs.[14,15,23]

In the high-frequency region, there are four optical modes in 1LM,[21] *i.e.*, A$''_2$ at ~290 cm^{-1}, E′ at ~235 cm^{-1}, A$'_1$ at ~172 cm^{-1} and E″ at ~119 cm^{-1}, where the A$''_2$ mode is Raman inactive and cannot be observed in the Raman spectra, and other three modes are Raman active.[4,5] The E′ and A$'_1$ modes are observed in 1LM excited by a 647 nm laser, as shown in Fig. 1(c). The E″ mode is too weak to be observed here and can only be observed at specific laser wavelengths.[4]

In *N*LM, the in-phase (out-of-phase) atomic displacement of the nearest chalcogen atoms between the adjacent layers makes the adjacent layers uncoupled (coupled). In general, the

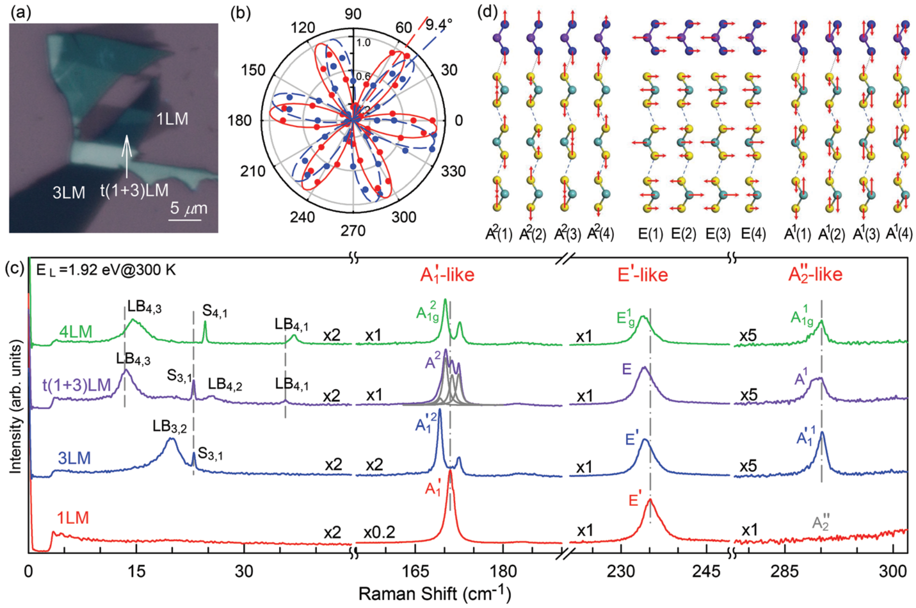

Fig. 1 (a) Optical images of the 1LM, 3LM, 4LM and t(1+3)LM. (b) The crystallographic–orientation dependent SHG intensity of 1LM (blue circle) and 3LM (red circle). (c) Raman spectra of 1LM, 3LM, 4LM and t(1+3)LM at RT. The vertical dashed lines are guides to eyes. Raman spectra are offset for clarity. (d) Schematic diagrams for the atomic displacements associated with the intralayer phonons at Γ point in t(1+3)LM, where the irreducible representations are indicated.

interlayer coupling leads to the splitting of each optical mode in 1LM into a set of N near-degenerate optical modes in NLM, *i.e.*, N Davydov entities in NLM corresponding to the phonon mode in 1LM.[3–5] Among the N Davydov entities, one mode involves all the uncoupled layers, which is named the uncoupled entity. The presence of coupled layers makes the frequency of other $N-1$ coupled entities higher than that of the uncoupled one. The same is true for the case in tMLM. Indeed, the Davydov entities in 3LM, 4LM and t(1+3)LM corresponding to the A_1' mode in 1LM are clearly observed in Fig. 1(c). The lattice symmetry of 3LM, 4LM and t(1+3)LM is different, resulting in different denotations for the corresponding Davydov entities. For example, the A_1' mode in 1LM gives rise to the A'^2_1 (R) and A''_2 (IR) modes in 3LM and the A^2_{1g} (R) and A_{2u} (IR) modes in 4LM, in which R and IR indicate the Raman and infrared activity. The A'^2_1 modes in 3LM and the A^2_{1g} mode in 4LM exhibit obvious Davydov splitting. For simplicity, hereafter we denote the Davydov entities in NLM and t(m+n)LM corresponding to the A''_2, E', A_1' and E'' modes in 1LM as the A''_2-like, E'-like, A_1'-like and E''-like modes, respectively. In this case, the A_1'-like modes in ONLM include $\frac{N+1}{2}$ A_1'(R) modes and $\frac{N-1}{2}$ A''_2(IR) modes, and those in even N-layer MoTe$_2$ (ENLM) include $\frac{N}{2}$ A_{1g}(R) modes and $\frac{N}{2}$ A_{2u}(IR) modes, where A_1' and A_{1g} modes are observed in Fig. 1(c). No evident splitting of the E'-like mode in 3LM and 4LM is observed. The A''_2-like modes in 3LM and 4LM are observed in spite of the absence of the Raman-inactive A''_2 mode in 1LM.

The existence of a twist interface in tMLM leads to a lower lattice symmetry than its constituents. The phonons at Γ in t(m+m)LM and t(m+n)LM (m≠n) can be expressed by the irreducible representation of D_3 and C_3 point groups, respectively, *i.e.*, $\Gamma(D_3) = A_1(R) + A_2(IR) + E(R)$ and $\Gamma(C_3) = A(R) + E(R)$. Based on the C_3 symmetry of t(1+3)LM, its A_1'-like and A''_2-like modes can be assigned to the A^2 and A^1 modes, respectively. Meanwhile, the E'-like mode is assigned to the E mode. The schematic diagrams of atomic displacements of the out-of-plane and in-plane intralayer modes in t(1+3)LM are depicted in Fig. 1(d) based on the diatomic linear chain model (DCM) (see the ESI†).[10] As indicated by the fitting shown in Fig. 1(c), the A_1'-like modes of t(1+3)LM exhibit four Davydov entities. This implies that its twist interface leads to different electron–phonon coupling from its constituents due to the modified interlayer coupling at the interface and the change of lattice symmetry in t(1+3)LM. In addition, the A''_2-like mode in t(1+3)LM exhibits spectral broadening in comparison with the corresponding modes in NLM.

As the Raman peaks of TMD flakes are expected to exhibit a smaller full width half maximum (FWHM) at low temperature than at RT,[24] allowing us to obtain more details of the spectral profile, we subsequently performed resonance Raman spectroscopy measurements at 4 K. Before we give insights into peak positions of the intralayer modes of t(m+n)LM and their correlation with interfacial coupling between its constituents, we first focus on their interlayer S and LB modes which are directly linked to the interlayer and interfacial coupling in t(m+n)LM. The twist angles of t(1+1)LM and t(1+3)LM were characterized by the orientational dependence of the SHG of their two ONLM constituents, as indicated in Fig. S4 (see the ESI†) and Fig. 1(b), respectively. Fig. 2(a) shows the low-frequency Raman spectra of several t(m+n)LM and the corresponding NLM ($N = m + n$) at 4 K. The S mode in 3LM is observed at the same peak position in t(1+3)LM and t(2+3)LM. This suggests that the interfacial S coupling in t(m+n)LM is negligible at its twist interface, similar to the case of twisted multilayer graphenes[14] and related vdWHs.[16,22] The S mode in 2LM is too weak to be observed in t(1+2)LM and t(2+3)LM. Several LB modes are observed in t(m+n)LM and NLM, as labeled in Fig. 2(a), which exhibit broader spectral profiles than the S mode. ω(LB) of t(m+n)LM shows a redshift relative to that of the corresponding NLM, as indicated by the dashed lines in Fig. 2(a). The experimental frequencies of LB$_{N,N-j}$ modes of t(m+n)LM and NLM are summarized in Fig. 2(b), which can be well fitted by the LCM[15,16,22] with the interlayer coupling of $\alpha^{\perp}$(M) = 7.91 × 10^{19} N m^{-3} and a weaker interfacial coupling $\alpha^{\perp}$(I). The weaker $\alpha^{\perp}$(I) of 5.14 × 10^{19} N m^{-3}, 4.75 × 10^{19} N m^{-3}, 5.85 × 10^{19} N m^{-3}, and 5.32 × 10^{19} N m^{-3} in t(1+1)LM, t(1+2)LM, t(1+3)LM and t(2+3)LM, respectively, lead to smaller ω(LB) in t(m+n)LM than that of the corresponding NLM.

Based on the obtained interlayer and interfacial coupling in t(m+n)LM, now we turn to understand the Davydov splitting of its out-of-plane intralayer modes at 4 K. Fig. 3(a) shows Raman spectra of the A_1'-like modes in t(m+n)LM and NLM. The dashed lines indicate the fitted Davydov entities, which were labeled according to their irreducible representation based on lattice symmetry. The Davydov entities in t(m+n)LM exhibit different frequencies from the corresponding entities in NLM. For example, the A^2_2 mode in t(1+1)LM shows a slight blueshift

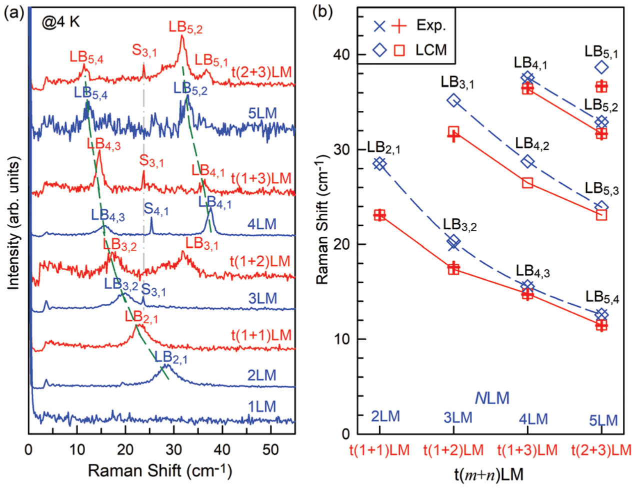

Fig. 2 (a) Raman spectra of t(m+n)LM and corresponding NLM ($N = m + n$) at 4 K in the region of 0–50 cm^{-1}. (b) The calculated frequencies in 2LM–5LM (blue open squares) and corresponding t(m+n)LM (red open diamonds) based on LCM. The experimental ones of the LB modes are also shown as crosses.

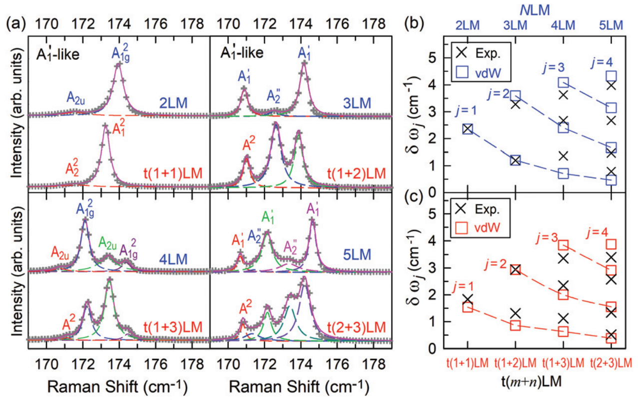

Fig. 3 (a) The Raman spectra of A_1'-like modes in t(*m*+*n*)LM and corresponding *NLM* ($N = m + n$) at 4 K in the region of 169–179 cm^{-1} (gray crosses) and the corresponding fitting results (dashed lines). Raman spectra are offset for clarity. The corresponding experimental (black crosses) and calculated (open squares) frequency differences between each Davydov entity and the uncoupled one in 2LM–5LM (b) and t(*m*+*n*)LM (c).

relative to the A_{2u} mode in 2LM; however, the A_1^2 mode in t(1+1)LM shows a significant redshift with respect to the A_{1g}^2 mode in 2LM. This indicates that the A_1'-like modes in t(m+n)LM and corresponding (m+n)LM exhibit different Davydov splitting, which may result from the interfacial LB coupling in t(m+n)LM different from the interlayer LB coupling in (m+n)LM.

As shown in Fig. 3(a), the observed Davydov splitting of the intralayer modes in t(m+n)LM and (m+n)LM is small and on the order of 1.0 cm^{-1}, which results from a small perturbation of the intralayer modes by the weak interlayer interaction.[5] The square of the interlayer mode frequency is directly proportional to the interlayer force constant. The interlayer mode is a direct signature for the interlayer interaction. In the case of first order approximation, the relation of the frequencies of the j^{th} coupled entity (ω_{cj}), the j^{th} interlayer mode ($\Delta\omega_j$) and uncoupled entity (ω_0) is as follows:

$$\omega_{cj}{}^2 = \omega_0{}^2 + (\Delta\omega_j)^2, \qquad (1)$$

where j = 1, 2,… and $N - 1$. For the out-of-plane intralayer modes in t(m+n)LM or NLM, $\Delta\omega_j = \omega(\mathrm{LB}_{N,N-j})$. Based on the DCM,[10] for the j^{th} coupled entity, atomic displacements of the nearest Te atoms between the adjacent layers is similar to that of the $\mathrm{LB}_{N,N-j}$ mode. The so-called vdW model[5] has been successfully used to understand the Davydov splitting of the A_1'-like modes in NLM at RT. In contrast to the results measured at RT,[5] all the N Davydov entities of NLM (N = 2, 3, 4, 5) are clearly distinguished at 4 K regardless of their Raman or infrared activity, as shown in Fig. 3(a). This may be due to the complex exciton resonance behavior.[5] Based on the vdW model and all the calculated ω(LB) of t(m+n)LM and NLM in Fig. 2(b), the frequencies of the Davydov entities of the corresponding A_1'-like modes can be calculated for both t(m+n)LM and NLM. The calculated frequency difference ($\delta\omega_j$) between the coupled entities (ω_{cj}) and uncoupled entity (ω_0) in t(m+n)LM and NLM is depicted in Fig. 3(b) and (c), respectively. The calculated $\delta\omega_j$ in t(m+n)LM and (m+n)LM agree with the experimental results. Based on the vdW model,

$$\delta\omega_j \approx (\omega(\mathrm{LB}_{N,N-j}))^2/2\omega_0. \qquad (2)$$

The larger the $\omega(\mathrm{LB}_{N,N-j})$, the larger the $\delta\omega_j$. Because $\omega(\mathrm{LB}_{N,N-j})$ in t(m+n)LM is smaller than that in (m+n)LM, $\delta\omega_j$ in t(m+n)LM should be smaller than that in (m+n)LM. Indeed, in t(1+3)LM, the experimental $\delta\omega_1$, $\delta\omega_2$ and $\delta\omega_3$ are 1.12 cm^{-1}, 2.34 cm^{-1} and 3.36 cm^{-1}, respectively, exhibiting an obvious decrease in comparison with those ($\delta\omega_1$ = 1.36 cm^{-1}, $\delta\omega_2$ = 2.67 cm^{-1} and $\delta\omega_3$ = 3.63 cm^{-1}) in (m+n)LM.

Because $\omega(A_2'')$ is larger than $\omega(A_1')$ in 1LM, Davydov splitting of the A_2''-like modes is much smaller than that of the A_1'-like modes in NLM. Moreover, Raman peaks of NLM at RT are expected to be much broader than those at low temperature.[24] The two factors make it difficult to distinguish the Davydov entities of the A_2''-like modes in NLM at RT. Therefore, unresolved spectral profiles were observed for the A_2''-like modes in NLM in previous reports, which are simply ascribed to the surface effects rather than Davydov splitting.[4,25] However, at 4 K, the resonance Raman spectra of the A_2''-like modes show evident splitting in NLM and t(m+n)LM, as indicated in Fig. 4(a). In particular, two and three Davydov entities are clearly distinguished in 2LM and 3LM, respectively, which is similar to the case of the corresponding A_1'-like modes. The A_2''-like modes in 4LM and 5LM also exhibit complex spectral profiles. Similar results are observed in t(m+n)LM. We use N Lorentzian peaks with similar FWHM to fit the A_2''-like modes in t(m+n)LM and NLM ($N = m + n$), as indicated by the dashed lines in Fig. 4(a). Only one peak is observed in t(1+1)LM. The absence of the A_2''-like mode at a lower frequency in t(1+1)LM

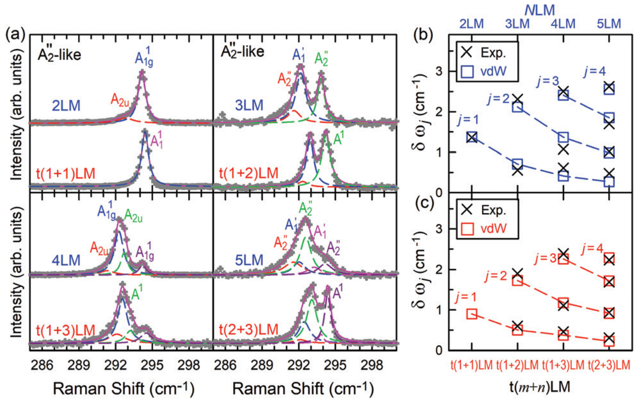

Fig. 4 (a) The Raman spectra of A_2''-like modes in t(*m*+*n*)LM and corresponding *NLM* ($N = m + n$) at 4 K in the region of 285–300 cm^{-1} (gray crosses) and the corresponding fitting results (dashed lines). Raman spectra are offset for clarity. The corresponding experimental (black crosses) and calculated (open squares) frequency differences between each Davydov entity and the uncoupled one in 2LM–5LM (b) and t(*m*+*n*)LM (c).

may be due to its weak electron–phonon coupling. The $\delta\omega_j$ in NLM and t(m+n)LM are calculated by using the vdW model, as summarized in Fig. 4(b) and (c), respectively. Good agreement between the calculated and experimental $\delta\omega_j$ implies the splitting components of the A_2''-like modes in t(m+n)LM and (m+n)LM are actually the Davydov entities. Similar to the A_1'-like modes, the A_2''-like modes in t(m+n)LM exhibit smaller Davydov splitting than in (m+n)LM, implying a weaker interfacial coupling between the constituents of t(m+n)LM than the interlayer coupling in (m+n)LM. It is worth noting that the Davydov splitting of the A_2''-like modes (Fig. 4(b and c)) is always smaller than the corresponding Davydov splitting of the A_1'-like modes (Fig. 3(b and c)) in the same sample, no matter in NLM or t(m+n)LM, indeed, as expected by eqn (2) because the frequency of the A_2''-like modes is higher than that of the A_1'-like modes.

Based on the knowledge of the impact of the interfacial coupling on the Davydov splitting of the out-of-plane intralayer modes in t(m+n)LM, now we turn to the influence of the weak interfacial S coupling on the in-plane intralayer modes, *i.e.*, the E′-like mode (~235 cm^{-1}). The frequency of the E′-like mode in NLM decreases with increasing layer numbers, similar to the case of other N-layer TMD flakes.[11] The broad peak at ~247 cm^{-1} appears in all the spectra of t(m+n)LM, mLM and nLM and can be attributed to the second-order Raman scattering of $A_{1g}(M)$ + LA(M),[26] as marked by asterisks in Fig. 5(a). Different from obvious Davydov splitting in A_2''-like and A_1'-like modes, even at 4 K, Davydov entities of the E′-like mode cannot be resolved in the Raman spectra of all the samples. t(2+3)LM exhibits the smallest FWHM while t(1+3)LM exhibits the largest FWHM among all the samples, which cannot be understood by the unresolved Davydov entities in these samples. The frequency of the E′-like mode in t(1+1)LM is identical to that of the corresponding mode in 1LM. To understand this peculiar property of the in-plane intralayer modes in t(1+1)LM, we apply the vdW model described by eqn (1). Because the intralayer S coupling between nLM and mLM is negligible in t(m+n)LM as discussed above, the E′-like mode in t(m+n)LM can be considered as the sum of the corresponding modes in its constituents, *i.e.*, mLM and nLM. Indeed, the spectral profile of the E′-like mode in t(m+n)LM can be fitted by those of the corresponding modes in nLM and mLM. This leads to the largest FWHM (~2.8 cm^{-1}) of the E′-like mode in t(1+3)LM among all the samples since the frequency difference of the E′-like modes between mLM and nLM reaches its maximum in t(1+3)LM, as shown in Fig. 5(a). The above results suggest that the in-plane intralayer modes in t(m+n)LM are localized within its constituents, similar to the case of the corresponding interlayer S modes (Fig. 1(c)).

From the above analysis, it is found that the interfacial coupling in t(m+n)LM dominates the spectral profile or Davydov splitting of the intralayer modes in t(m+n)LM. In twisted TMD multilayers, the twist angle is another important degree of freedom to manipulate the interfacial coupling, especially when the twist angle is close to the magic angle.[17,27–33] To investigate how the twist angle beyond the magic angle would modify the interfacial coupling and the intralayer modes in t(m+n)LM, we also measured the resonance Raman spectra of t(1+3)LM with different twist angles in the range of 9°–20° (see Fig. S5 in the ESI†), as plotted in Fig. 5(b). The $LB_{4,3}$ modes in all t(1+3)LM exhibit almost the same frequency, which indicates that interfacial LB coupling is independent on the twist angle in this range. Meanwhile, there is also no obvious frequency shift in any Davydov component of the A_1'-like modes, which further confirms the identical interfacial coupling among these samples. However, the relative Raman intensity between different Davydov entities significantly varies with the twist angle, which can be ascribed to the modulation of the electron–phonon coupling by the twist angle. Further investigations need to figure out the physics behind this interesting phenomenon, which is beyond the scope of this work.

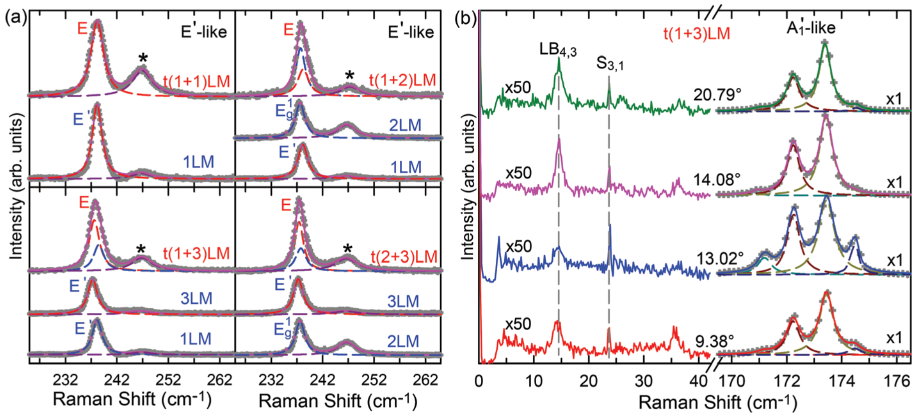

Fig. 5 (a) The Raman spectra of E′-like modes in t(m+n)LM and its constituents mLM and nLM at 4 K in the region of 225–265 cm^{-1} (gray crosses) and the fitting results (dashed lines). Raman spectra are offset for clarity. (b) Raman spectra of t(1+3)LM with different twist angles at 4 K in the ultra-low-frequency region (0–50 cm^{-1}) and 170–176 cm^{-1}.

4. Conclusions

In summary, the interlayer and intralayer modes of *N*LM and tMLM are investigated by high-resolution resonance Raman spectroscopy at a low temperature of 4 K. All the *N* Davydov entities of the A_1'-like and A_2''-like modes in *N*LM and tMLM are observed. On the other hand, the spectral profile of the E′-like modes in tMLM is the sum of those from the corresponding constituents. All the spectral features can be well understood using the vdW model. The frequency differences between the Davydov entities of the A_1'-like and A_2''-like modes can be reproduced once the interlayer LB coupling in *N*LM and interfacial LB coupling in tMLM are considered, while the E′-like mode in tMLM is localized within its constituents due to its negligible interfacial S coupling. This study promotes the understanding of the effect of interlayer/interfacial coupling on the in-plane and out-of-plane intralayer modes in twisted TMD multilayers and will motivate related studies of Davydov splitting in other twisted materials and the related vdWHs.

Author contributions

P.-H. Tan conceived the idea, directed and supervised the project. Y.-C. Leng and P.-H. Tan designed the experiments. Y.-C. Leng performed experiments. Y. Zhou and H. Li prepared the samples. Y.-C. Leng, M.-L. Lin and P.-H. Tan analyzed the data with inputs from J.-B. Wu, D. Meng and X. Cong; Y.-C. Leng, M.-L. Lin and P.-H. Tan wrote the manuscript with input from all authors.

Conflicts of interest

There are no conflicts to declare.

Acknowledgements

We acknowledge support from the National Key Research and Development Program of China (Grant No. 2016YFA0301204), the National Natural Science Foundation of China (Grant No. 12004377, 11874350 and 21571101), the CAS Key Research Program of Frontier Sciences (Grant No. ZDBS-LY-SLH004) and the China Postdoctoral Science Foundation (Grant No. 2019TQ0317).

References

1 P. H. Tan, W. P. Han, W. J. Zhao, Z. H. Wu, K. Chang, H. Wang, Y. F. Wang, N. Bonini, N. Marzari, N. Pugno, G. Savini, A. Lombardo and A. C. Ferrari, *Nat. Mater.*, 2012, **11**, 294–300.

2 X. Zhang, Q.-H. Tan, J.-B. Wu, W. Shi and P.-H. Tan, *Nanoscale*, 2016, **8**, 6435–6450.

3 P. N. Ghosh and C. R. Maiti, *Phys. Rev. B: Condens. Matter Mater. Phys.*, 1983, **28**, 2237–2239.

4 G. Froehlicher, E. Lorchat, F. Fernique, C. Joshi, A. Molina-Sánchez, L. Wirtz and S. Berciaud, *Nano Lett.*, 2015, **15**, 6481–6489.

5 Q. J. Song, Q. H. Tan, X. Zhang, J. B. Wu, B. W. Sheng, Y. Wang, Q. X. Wang, L. Dai and P. H. Tan, *Phys. Rev. B*, 2016, **93**, 115409.

6 K. Kim, J.-U. Lee, D. Nam and H. Cheong, *ACS Nano*, 2016, **10**, 8113–8120.

7 M. Grzeszczyk, K. Gołasa, M. Zinkiewicz, K. Nogajewski, M. R. Molas, M. Potemski, A. Wysmołek and A. Babiński, *2D Mater.*, 2016, **3**, 025010.

8 W. Na, K. Kim, J.-U. Lee and H. Cheong, *2D Mater.*, 2018, **6**, 015004.

9 A. Molina-Sanchez and L. Wirtz, *Phys. Rev. B: Condens. Matter Mater. Phys.*, 2011, **84**, 155413.

10 X. Zhang, W.-P. Han, J.-B. Wu, S. Milana, Y. Lu, Q.-Q. Li, A. C. Ferrari and P.-H. Tan, *Phys. Rev. B: Condens. Matter Mater. Phys.*, 2013, **87**, 115413.

11 C. Lee, H. Yan, L. E. Brus, T. F. Heinz, J. Hone and S. Ryu, *ACS Nano*, 2010, **4**, 2695–2700.

12 W. Zhao, Z. Ghorannevis, K. K. Amara, J. R. Pang, M. Toh, X. Zhang, C. Kloc, P. H. Tan and G. Eda, *Nanoscale*, 2013, **5**, 9677–9683.

13 Q.-H. Tan, X. Zhang, X.-D. Luo, J. Zhang and P.-H. Tan, *J. Semicond.*, 2017, **38**, 031006.

14 J.-B. Wu, X. Zhang, M. Ijäs, W.-P. Han, X.-F. Qiao, X.-L. Li, D.-S. Jiang, A. C. Ferrari and P.-H. Tan, *Nat. Commun.*, 2014, **5**, 5309.

15 J.-B. Wu, Z.-X. Hu, X. Zhang, W.-P. Han, Y. Lu, W. Shi, X.-F. Qiao, M. Ijiäs, S. Milana, W. Ji, A. C. Ferrari and P.-H. Tan, *ACS Nano*, 2015, **9**, 7440–7449.

16 M.-L. Lin, Y. Zhou, J.-B. Wu, X. Cong, X.-L. Liu, J. Zhang, H. Li, W. Yao and P.-H. Tan, *Nat. Commun.*, 2019, **10**, 2419.

17 K. Liu, L. Zhang, T. Cao, C. Jin, D. Qiu, Q. Zhou, A. Zettl, P. Yang, S. G. Louie and F. Wang, *Nat. Commun.*, 2014, **5**, 1–6.

18 H. Li, J. Wu, X. Huang, Z. Yin, J. Liu and H. Zhang, *ACS Nano*, 2014, **8**, 6563–6570.

19 Y. Li, Y. Rao, K. F. Mak, Y. You, S. Wang, C. R. Dean and T. F. Heinz, *Nano Lett.*, 2013, **13**, 3329–3333.

20 C. Ruppert, O. B. Aslan and T. F. Heinz, *Nano Lett.*, 2014, **14**, 6231–6236.

21 X. Zhang, X.-F. Qiao, W. Shi, J.-B. Wu, D.-S. Jiang and P.-H. Tan, *Chem. Soc. Rev.*, 2015, **44**, 2757–2785.

22 H. Li, J.-B. Wu, F. Ran, M.-L. Lin, X.-L. Liu, Y. Zhao, X. Lu, Q. Xiong, J. Zhang, W. Huang, H. Zhang and P.-H. Tan, *ACS Nano*, 2017, **11**, 11714–11723.

23 M.-L. Lin, Q.-H. Tan, J.-B. Wu, X.-S. Chen, J.-H. Wang, Y.-H. Pan, X. Zhang, X. Cong, J. Zhang, W. Ji, P.-A. Hu, K.-H. Liu and P.-H. Tan, *ACS Nano*, 2018, **12**, 8770–8780.

24 G. P. Srivastava and I. O. Thomas, *Phys. Rev. B*, 2018, **98**, 035430.

25 M. Grzeszczyk, K. Gołasa, M. R. Molas, K. Nogajewski, M. Zinkiewicz, M. Potemski, A. Wysmołek and A. Babiński, *Sci. Rep.*, 2018, **8**, 17745.

26 H. Guo, T. Yang, M. Yamamoto, L. Zhou, R. Ishikawa, K. Ueno, K. Tsukagoshi, Z. Zhang, M. S. Dresselhaus and R. Saito, *Phys. Rev. B: Condens. Matter Mater. Phys.*, 2015, **91**, 205415.

27 S. Huang, X. Ling, L. Liang, J. Kong, H. Terrones, V. Meunier and M. S. Dresselhaus, *Nano Lett.*, 2014, **14**, 5500–5508.

28 A. M. van der Zande, J. Kunstmann, A. Chernikov, D. A. Chenet, Y. You, X. Zhang, P. Y. Huang, T. C. Berkelbach, L. Wang, F. Zhang, M. S. Hybertsen, D. A. Muller, D. R. Reichman, T. F. Heinz and J. C. Hone, *Nano Lett.*, 2014, **14**, 3869–3875.

29 S. Huang, L. Liang, X. Ling, A. A. Puretzky, D. B. Geohegan, B. G. Sumpter, J. Kong, V. Meunier and M. S. Dresselhaus, *Nano Lett.*, 2016, **16**, 1435–1444.

30 M. H. Naik and M. Jain, *Phys. Rev. Lett.*, 2018, **121**, 266401.

31 A. Weston, Y. Zou, V. Enaldiev, A. Summerfield, N. Clark, V. Zólyomi, A. Graham, C. Yelgel, S. Magorrian, M. Zhou, J. Zultak, D. Hopkinson, A. Barinov, T. H. Bointon, A. Kretinin, N. R. Wilson, P. H. Beton, V. I. Fal'ko, S. J. Haigh and R. Gorbachev, *Nat. Nanotechnol.*, 2020, **15**, 592–597.

32 A. A. Puretzky, L. Liang, X. Li, K. Xiao, B. G. Sumpter, V. Meunier and D. B. Geohegan, *ACS Nano*, 2016, **10**, 2736–2744.

33 J. Quan, L. Linhart, M.-L. Lin, D. Lee, J. Zhu, C.-Y. Wang, W.-T. Hsu, J. Choi, J. Embley, C. Young, T. Taniguchi, K. Watanabe, C.-K. Shih, K. Lai, A. H. MacDonald, P.-H. Tan, F. Libisch and X. Li, *Nat. Mater.*, 2021, DOI: 10.1038/s41563-021-00960-1.

Electronic Supplementary Information
Intrinsic effect of interfacial coupling on the high-frequency intralayer modes in twisted multilayer MoTe$_2$

Yu-Chen Leng,[ab] Miao-Ling Lin,[a] Yu Zhou,[c] Jiang-Bin Wu,[a] Da Meng,[a] Xin Cong,[ab] Hai Li,[c] and Ping-Heng Tan*[abd]

Diatomic Chain Model for out-of-plane intralayer mode in N-layer MoTe$_2$

The schematic diagrams of atomic displacements of the out-of-plane intralayer modes in N-layer MoTe$_2$ (NLM) are obtained based on the diatomic linear chain model (DCM)[1]. Two force constants, α_{mt} and α_{tt} ,are needed to describe the vibration modes in NLM. α_{mt} represents the force constant per unit area between the nearest Mo and Te planes within a MoTe$_2$ layer and α_{tt} represents the force constant per unit area between two nearest Te planes in two adjacent layers. Since the Mo and Te atoms in the A'_1-like and A''_2-like modes vibrate perpendicular to the basal plane, only the perpendicular components of the force constants need to be considered. For simplicity, all the following α_{mt} and α_{tt} represent the perpendicular components of the corresponding force constants. $\alpha_{tt} = 7.91 \times 10^{19} N/m^3$ can be obtained by the frequency of the layer-breathing (LB) modes, as described in main text. α_{mt} can be calculated from the frequency of the A'_1 mode in 1LM:

The vibrations of the three atoms in 1LM can be described by the following equations,

$$\begin{cases} m_{\text{Te}}\ddot{U}_{\text{Te1}} = -\alpha_{mt}\ddot{U}_{\text{Te1}} + \alpha_{mt}\ddot{U}_{\text{Mo}} \\ m_{\text{Mo}}\ddot{U}_{\text{Mo}} = \alpha_{mt}\ddot{U}_{\text{Te1}} - 2\alpha_{mt}\ddot{U}_{\text{Mo}} + \alpha_{mt}\ddot{U}_{\text{Te2}} \\ m_{\text{Te}}\ddot{U}_{\text{Te2}} = \alpha_{mt}\ddot{U}_{\text{Mo}} - \alpha_{mt}\ddot{U}_{\text{Te2}} \end{cases} \tag{S1}$$

where m_{Te} and m_{Mo} represent the mass of Te and Mo atoms, respectively. U_{Te} and U_{Mo} represent the displacements of the Te and Mo atoms relative to their corresponding equilibrium positions, respectively, subscripts 1 and 2 are used to distinguish the two different Te atoms in one layer. The solution of the above equations of motion is obtained by using the following substitution,

$$U = u \times e^{-i\omega t} \tag{S2}$$

where u is the amplitude of displacement of one atom, and ω represent its vibration frequency. After the substitution, the following equations are obtained,

$$\begin{cases} \omega^2 u_{\text{Te1}} = -\dfrac{\alpha_{mt}}{m_{\text{Te}}} u_{\text{Te1}} + \dfrac{\alpha_{mt}}{m_{\text{Te}}} u_{\text{Mo}} \\ \omega^2 u_{\text{Mo}} = \dfrac{\alpha_{mt}}{m_{\text{Mo}}} u_{\text{Te1}} - 2\dfrac{\alpha_{mt}}{m_{\text{Mo}}} u_{\text{Mo}} + \dfrac{\alpha_{mt}}{m_{\text{Mo}}} u_{\text{Te2}} \\ \omega^2 u_{\text{Te2}} = \dfrac{\alpha_{mt}}{m_{\text{Te}}} u_{\text{Mo}} - \dfrac{\alpha_{mt}}{m_{\text{Te}}} u_{\text{Te2}} \end{cases} \tag{S3}$$

which can be expressed in a matrix form as,

$$\omega^2 \mathbf{u} = \mathbf{D}\mathbf{u}. \tag{S4}$$

---

[a] *State Key Laboratory of Superlattices and Microstructures, Institute of Semiconductors, Chinese Academy of Sciences, Beijing 100083, China.*
E-mail: phtan@semi.ac.cn
[b] *Center of Materials Science and Optoelectronics Engineering & CAS Center of Excellence in Topological Quantum Computation, University of Chinese Academy of Sciences, Beijing 100049, China.*
[c] *Key Laboratory of Flexible Electronics and Institute of Advanced Materials, Jiangsu National Synergetic Innovation Center for Advanced Materials, Nanjing Tech University, 30 South Puzhu Road, 211816 Nanjing, China.*
[d] *Beijing Academy of Quantum Information Science, Beijing 100193, China.*

This equation is equivalent to

$$2\pi^2 c^2 \omega^2 \mathbf{u}' = \mathbf{D}\mathbf{u}' \tag{S5}$$

where c $= 3 \times 10^8$ m/s is the speed of light, $\mathbf{u}'$ is the column vector of displacement and $\mathbf{D}$ is a force constant matrix:

$$\mathbf{D} = \begin{pmatrix} -\frac{\alpha_{mt}}{\mu_{\mathrm{Te}}} & \frac{\alpha_{mt}}{\mu_{\mathrm{Te}}} & 0 \\ \frac{\alpha_{mt}}{\mu_{\mathrm{Mo}}} & -2\frac{\alpha_{mt}}{\mu_{\mathrm{Mo}}} & \frac{\alpha_{mt}}{\mu_{\mathrm{Mo}}} \\ 0 & \frac{\alpha_{mt}}{\mu_{\mathrm{Te}}} & -\frac{\alpha_{mt}}{\mu_{\mathrm{Te}}} \end{pmatrix}. \tag{S6}$$

Here, $\mu_{\mathrm{Te}} = 2.03 \times 10^{-6}$ kg/m^2 and $\mu_{\mathrm{Mo}} = 1.53 \times 10^{-6}$ kg/m^2 are the mass of Te and Mo atoms per unit area, respectively. For the A_1' mode of 1LM, the Mo atom do not vibrate, giving $\omega(A_1') = \frac{1}{\sqrt{2}\pi c}\sqrt{\frac{\alpha_{mt}}{\mu_{\mathrm{Te}}}}$.[1] We measure $\omega(A_1') \sim 172.8$ cm^{-1} in 1LM. This gives $\alpha_{mt} = 2.15 \times 10^{21}$ N/m^3.

For *N*LM, the corresponding force constant matrix can be given by a similar method. For example, the force constant matrix D for 2LM can be written as:

$$\mathbf{D} = \begin{pmatrix} -\frac{\alpha_{mt}}{\mu_{\mathrm{Te}}} & \frac{\alpha_{mt}}{\mu_{\mathrm{Te}}} & 0 & 0 & 0 & 0 \\ \frac{\alpha_{mt}}{\mu_{\mathrm{Mo}}} & -2\frac{\alpha_{mt}}{\mu_{\mathrm{Mo}}} & \frac{\alpha_{mt}}{\mu_{\mathrm{Mo}}} & 0 & 0 & 0 \\ 0 & \frac{\alpha_{mt}}{\mu_{\mathrm{Te}}} & -\frac{\alpha_{mt}}{\mu_{\mathrm{Te}}} - \frac{\alpha_{tt}}{\mu_{\mathrm{Te}}} & \frac{\alpha_{tt}}{\mu_{\mathrm{Te}}} & 0 & 0 \\ 0 & 0 & \frac{\alpha_{tt}}{\mu_{\mathrm{Te}}} & -\frac{\alpha_{tt}}{\mu_{\mathrm{Te}}} - \frac{\alpha_{mt}}{\mu_{\mathrm{Te}}} & \frac{\alpha_{mt}}{\mu_{\mathrm{Te}}} & 0 \\ 0 & 0 & 0 & \frac{\alpha_{mt}}{\mu_{\mathrm{Mo}}} & -2\frac{\alpha_{mt}}{\mu_{\mathrm{Mo}}} & \frac{\alpha_{mt}}{\mu_{\mathrm{Mo}}} \\ 0 & 0 & 0 & 0 & \frac{\alpha_{mt}}{\mu_{\mathrm{Te}}} & -\frac{\alpha_{mt}}{\mu_{\mathrm{Te}}} \end{pmatrix}, \tag{S7}$$

Then the displacement of each atom in A_1'-like and A_2''-like modes can be obtained by solving $\mathbf{u}$ in Eq. (S5). The results are summarized in Fig.S1 and S2.

Notes and references

1 X. Zhang, W.-P. Han, J.-B. Wu, S. Milana, Y. Lu, Q.-Q. Li, A. C. Ferrari and P.-H. Tan, *Phys. Rev. B*, 2013, **87**, 115413.

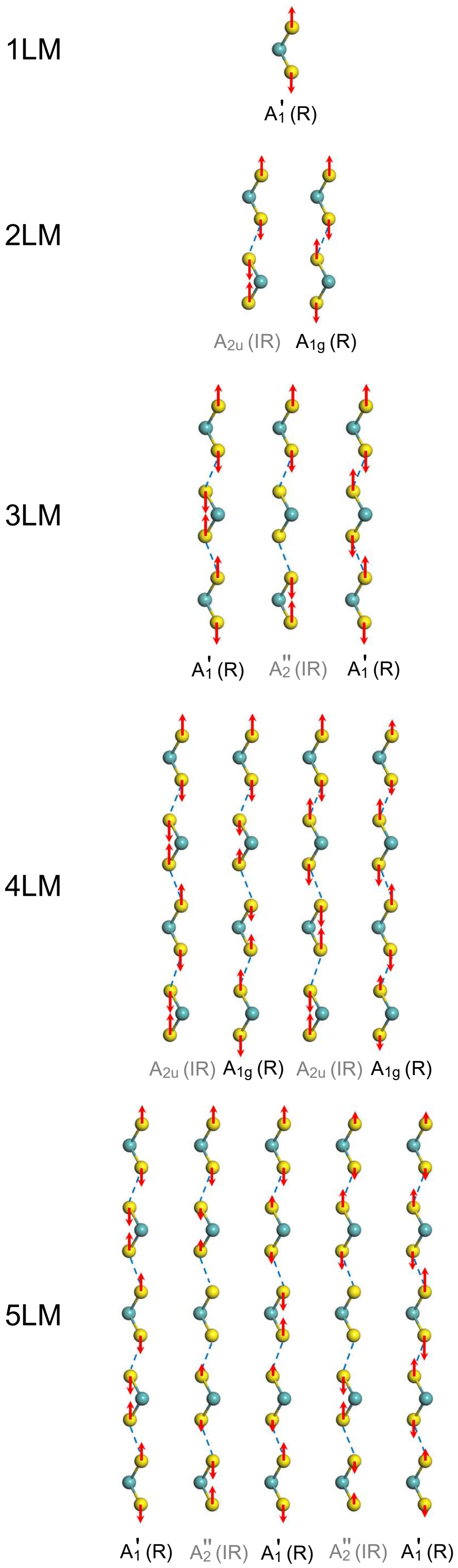

Fig. S1 Calculated atom displacements for the A_1'-like modes($\sim$172 cm^{-1}) in 1LM-5LM by DCM. The frequencies of the modes in each layer increase from left to right. The irreducible representation of each modes with Raman activity(black) and infrared activity(gray) are indicated. The directions and lengths of the arrows represent the directions and amplitudes of the atomic vibration, respectively.

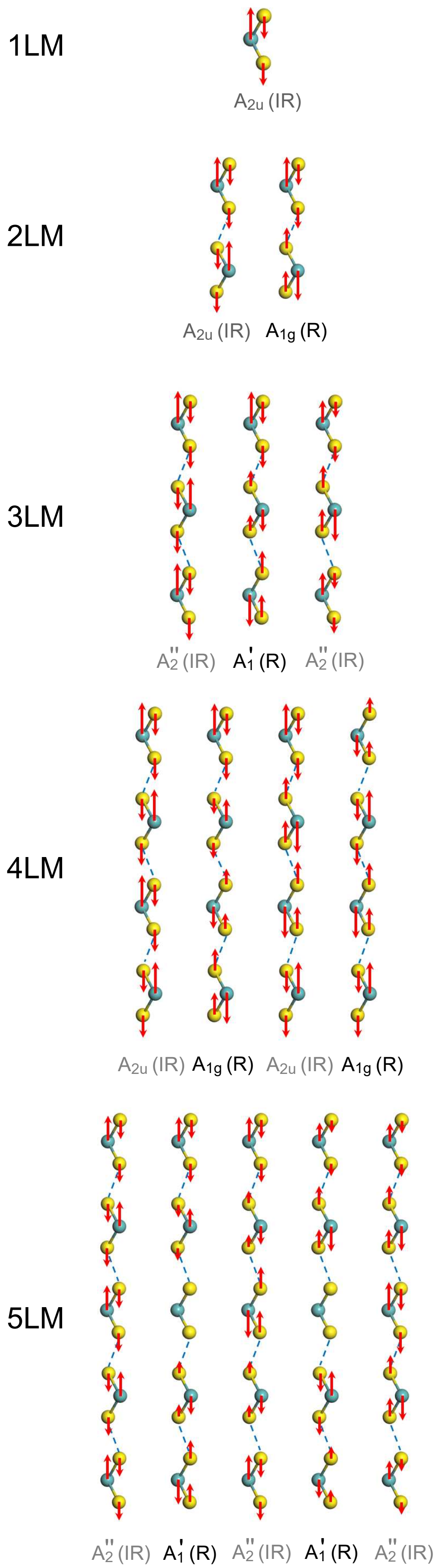

Fig. S2 Calculated atom displacements for the A_2''-like modes($\sim$290 cm^{-1}) in 1LM-5LM by DCM. The frequencies of the modes in each layer increase from left to right. The irreducible representation of each modes with Raman activity(black) and infrared activity(gray) are indicated. The directions and lengths of the arrows represent the directions and amplitudes of the atomic vibration, respectively.

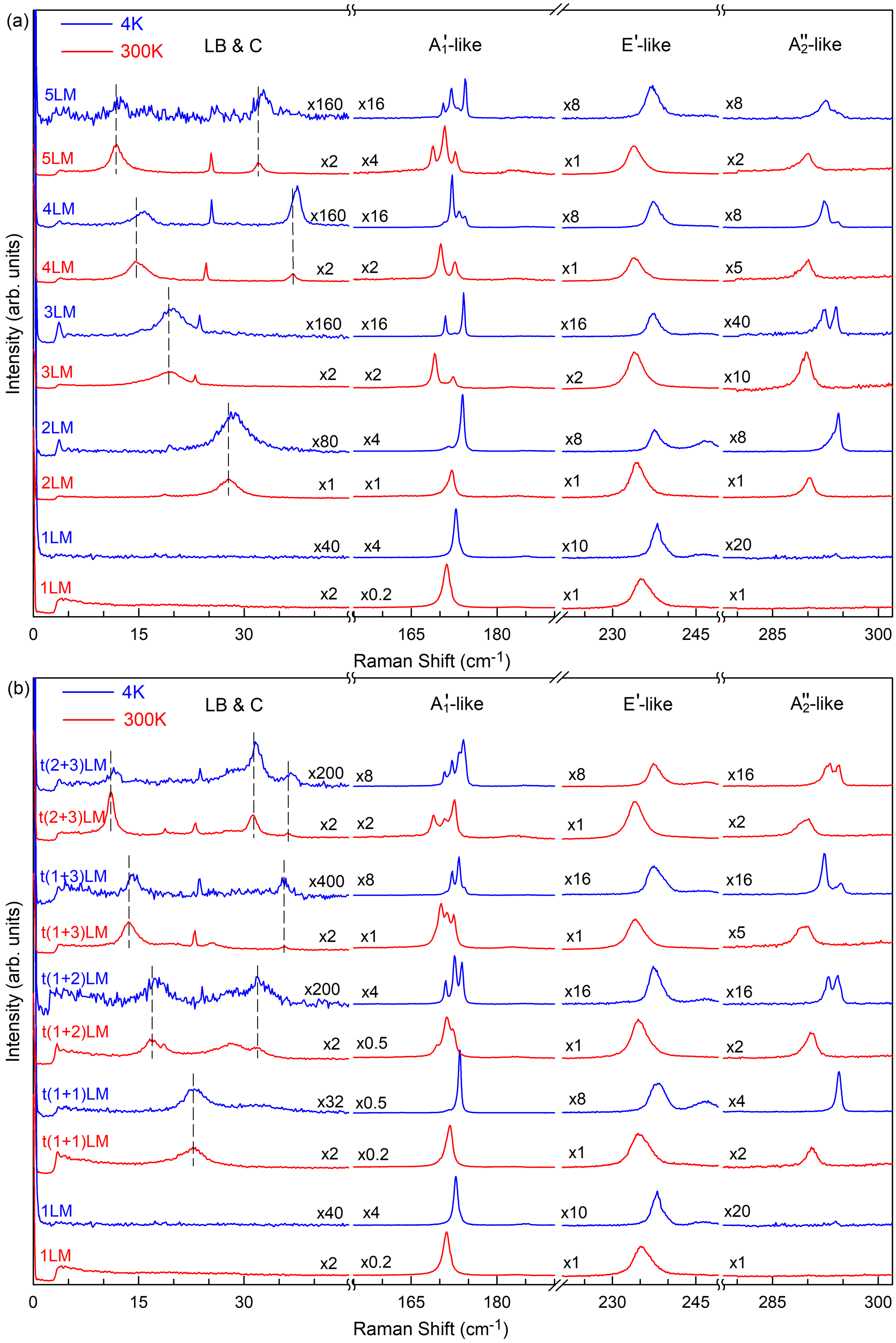

Fig. S3 The Raman spectra of interlayer and intralayer modes in (a) NLM and (b) $t(m+n)$LM at 4K (blue) and 300K (red). Raman spectra are offset for clarity.

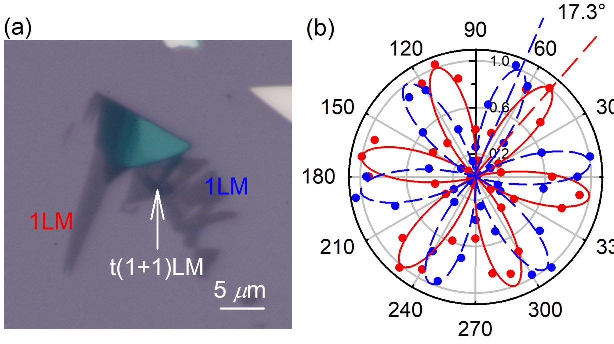

Fig. S4 (a) Optical image of the t(1+1)LM. (b) The crystallographic-orientation dependent SHG intensity of two 1LM constituents (blue circle and red circle).

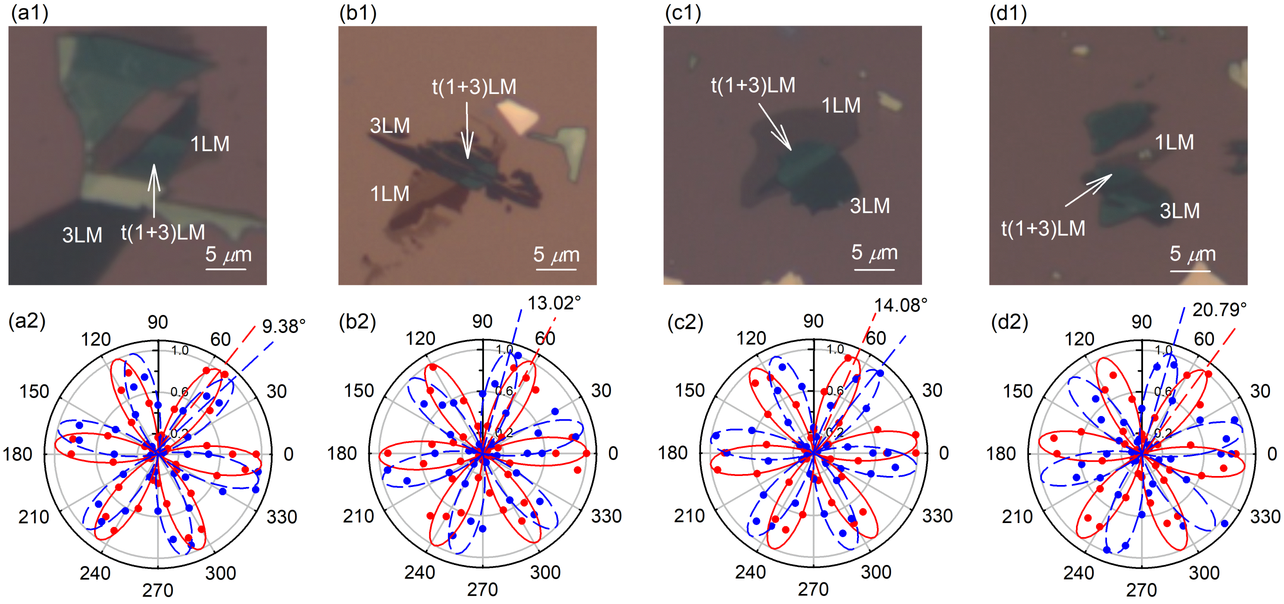

Fig. S5 (a1-d1) Optical image of four t(1+3)LM samples with different twist angles and (a2-d2) the crystallographic-orientation dependent SHG intensity of their 1LM (blue circle) and 3LM (red circle) constituents.

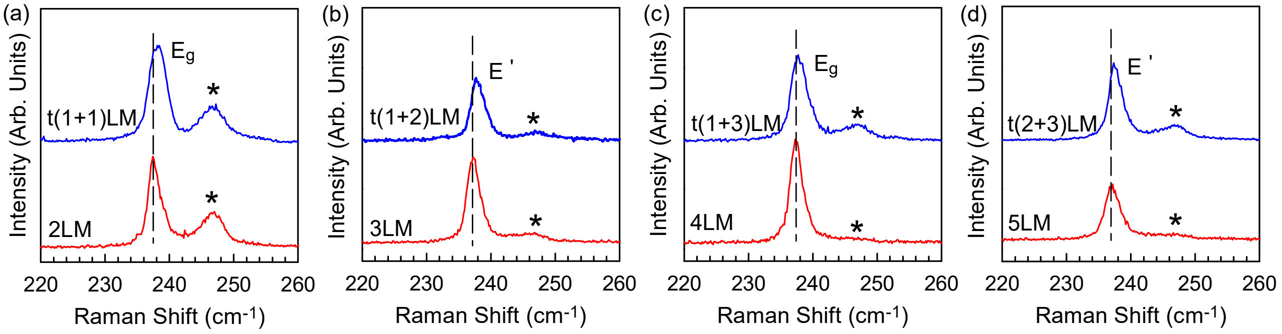

Fig. S6 Raman spectra of E'-like modes in $t(m+n)$LM and corresponding NLM ($N = m+n$): (a) t(1+1)LM and 2LM, (b) t(1+2)LM and 3LM, (c) t(1+3)LM and 4LM, (d) t(2+3)LM and 5LM. The combination modes, A_{1g}(M)+LA(M), are marked with asterisk. The vertical dashed lines are guides to eyes.